Nonlinear Modeling and Bifurcations in the Boost Converter

Soumitro Banerjee, *Member, IEEE,* and Krishnendu Chakrabarty

***Abstract*— Occurrence of nonlinear phenomena like subharmonics and chaos in power electronic circuits has been reported recently. In this paper, we investigate these phenomena in the current-mode-controlled boost converter. A nonlinear model in the form of a mapping from one point of observation to the next has been derived. The map has a closed form even when the parasitic elements are included. The bifurcation behavior of the boost converter has been investigated with the help of this discrete model.**

***Index Terms*—Boost converter, chaos, nonlinear phenomena.**

I. Introduction

IN RECENT times it has been observed that some power electronic (PE) circuits exhibit deterministic chaos [1]–[3], and it has been suspected that such phenomena may be responsible for the unusually high noise in some PE circuits. Naturally, what was so far branded under the single head "noise" in PE literature, may actually be due to deterministic nonlinear phenomena.

It has been demonstrated that current-mode-controlled buck converter and boost converter are prone to subharmonic behavior and chaos [4]–[6]. Still, very little information is available today on the parameter domains in which chaotic behavior may occur, and the possible pathways through which such systems may enter chaos. The work referred above only demonstrates the existence of chaotic mode of operation in the buck converter and the boost converter. Since these converters have wide industrial application, it becomes necessary to study the bifurcation phenomena in PE converters to understand the change of behavior as parameters are varied.

Such studies for the buck converter [7] have recently been reported. In this paper we present the studies on the bifurcation behavior of the current-mode-controlled boost converter.

Once it is recognized that the boost converter has nonlinear behavior, it becomes necessary to develop a nonlinear model of the system. The method currently in vogue in PE literature, the state-space averaging technique, does not serve this purpose and fails to explain the subharmonic modes and chaos in the boost converter. In view of this problem, [8] used a large-signal analysis of the continuous-time system while [9] proposed that discrete models should be developed for PE circuits as mappings of the form

$$\mathbf{x}_{n+1} = f(\mathbf{x}_n). \tag{1}$$

Such mappings, applied to the state space, would give the state of the system at a *switching instant* in terms of the previous one. A map-based model would disregard the dynamics between switching instants but would capture the nonlinearity since most PE circuits are piecewise linear, with nonlinear behavior contributed only by the switching discontinuity.

It was found, however, that closed-form expressions for the map can not be derived for most PE circuits. In such cases, the map has to be obtained numerically [9]. One welcome exception is the current-mode-controlled boost converter, where the map *can* be obtained in closed form. Such a map-based model for the boost converter was developed in [5] assuming idealized circuit elements.

When we checked the predictions of this map-based model against experiment and simulation of the continuous time model of the experimental setup, we found that the parasitic elements like the resistance of the inductor and capacitor have significant effects and their presence should not be ignored in a realistic model. In this paper we derive the model including the parasitic elements and show that it still retains a closed form. We also derive the map when observations are made at every *clock* instant (instead of every switching instant).

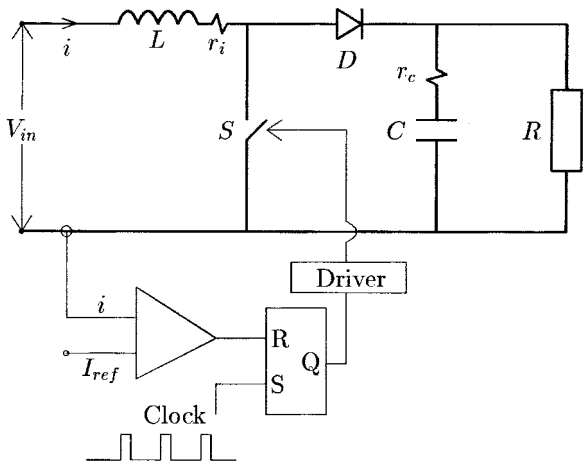

Fig. 1. Circuit diagram of the boost converter.

Manuscript received April 29, 1996; revised March 20, 1997. This work was supported by the Department of Science and Technology, Government of India, under Project III 4(23)/94-ET. Recommended by Associate Editor, R. L. Steigerwald.

S. Banerjee is with the Department of Electrical Engineering, Indian Institute of Technology, Kharagpur 721302, India (e-mail: soumitro@ee.iitkgp.ernet.in).

K. Chakrabarty is with the Department of Electrical Engineering, Regional Engineering College, Silchar 788010, India.

Publisher Item Identifier S 0885-8993(98)01954-1.

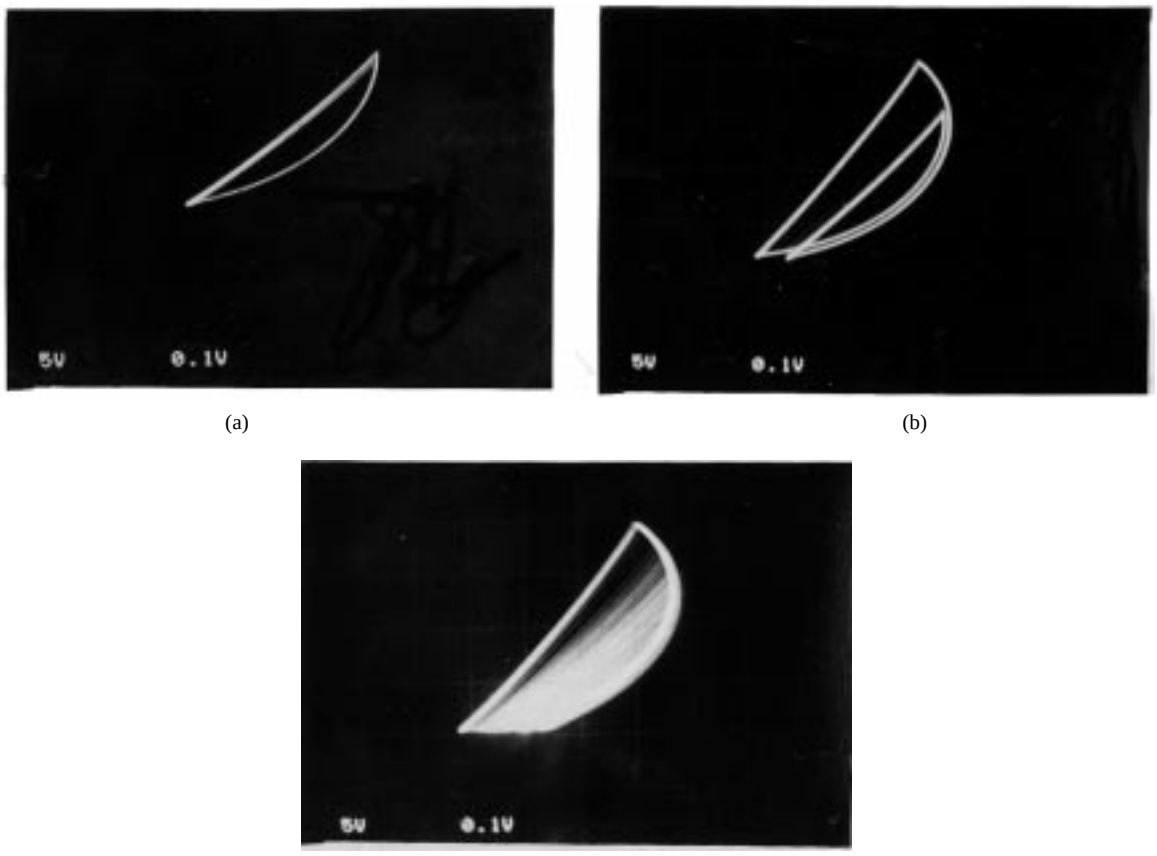

(a) (b)

(c)

Fig. 2. (a) Period 1 phase-plane trajectory of the boost converter. Parameter values are: $V_{in} = 42$ V, $R = 20\ \Omega$. (b) Period 2 phase-plane trajectory of the boost converter. Parameter values are: $V_{in} = 35$ V, $R = 20\ \Omega$. (c) Chaotic phase-plane trajectory of the boost converter. Parameter values are: $V_{in} = 20$ V, $R = 20\ \Omega$.

A. The Boost Converter

The boost converter circuit (Fig. 1) consists of a controlled switch S, an uncontrolled switch D, an inductor L, a capacitor C, and a load resistor R. The switching is controlled by a feedback path consisting of a comparator and a flip-flop. The comparator compares the current through the inductor and a reference current.

In a boost converter, the output voltage is always higher than the input voltage. When the controlled switch is turned on, the current flows through the inductor and energy is stored in it. When the controlled switch is turned off, the stored energy in the inductor drops and the polarity of the inductor voltage changes so that it adds to the input voltage. The voltage across the inductor and the input voltage together charge the output capacitor to a voltage higher than the input voltage. We assume continuous conduction mode (CCM), where the clock period and the value of the inductor are so chosen that the inductor current never falls to zero.

There are two states of the circuit depending on whether the controlled switch S is open or closed. When switch S is closed, the current through the inductor rises and any clock pulse arriving during that period is ignored. The switch S opens when i reaches the reference current I_{ref}. When switch S is open, the current i falls. The switch S closes again upon the arrival of the next clock pulse.

The system is governed by two sets of linear differential equations pertaining to the *on* and *off* states of the controlled switch. The output voltage v_c and the inductor current i are taken as state variables. During the "on" period the equations are

$$\frac{di}{dt} = \frac{V_{in}}{L} - \frac{r_i}{L}\, i \tag{2}$$

$$\frac{dv_c}{dt} = -\frac{v_c}{C(R+r_c)}. \tag{3}$$

And the state equations during "off" period are

$$\frac{di}{dt} = \frac{V_{in}}{L} - \frac{i}{L}\left(r_i + \frac{Rr_c}{R+r_c}\right) - v_c\,\frac{R}{L(R+r_c)} \tag{4}$$

$$\frac{dv_c}{dt} = \frac{1}{C(R+r_c)}\,(Ri - v_c) \tag{5}$$

where the parasitic elements r_i and r_c are the resistance of the inductor and capacitor, respectively. The switching between the two sets of equations is governed by the above feedback process.

A few experimentally observed trajectories in the phase-plane (the inductor current versus output voltage) is shown in Fig. 2. The nominal values of the fixed parameters are $L = 27$ mH, $C = 120\ \mu$F, $R = 20\ \Omega$, $r_c = 0.2\ \Omega$, $r_l = 0.9\ \Omega$ and clock frequency 500 Hz. Three cases are shown: period 1 (for

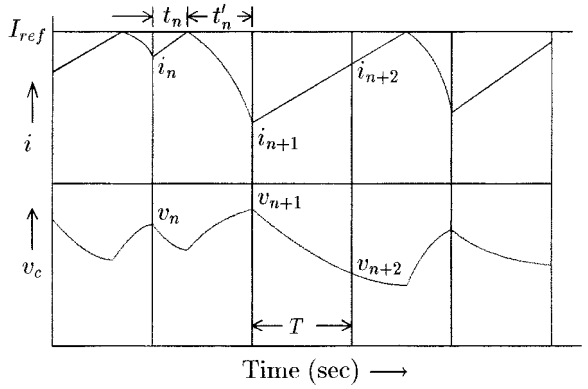

Fig. 3. Time plot of output voltage and inductor current of the boost converter with clock pulses.

$V_{in} = 42$ V), period 2 (for $V_{in} = 35$ V), and chaos (for $V_{in} = 20$ V).

II. The Map-Based Model for the Boost Converter

In this section, we first derive an expression for the mapping from one switching instant to the next in the $\mathbb{R}^2$ space formed by v_c and i. It would hold under the following assumptions.

1) The value of the inductor and the switching frequency are so chosen that there is no discontinuous conduction.
2) The value of the capacitance is so chosen that the output voltage v_c does not go below the input voltage at any part of the cycle.[1]

Fig. 3 shows the typical behavior of the state variables along with the clock pulses. We take the closure of the control switch as $t = 0$. At this time let the initial conditions be $i = i_n$ and $v_c = v_n$.

The switch turns off when the current i in the inductor reaches reference current $I_{\rm ref}$. The on-time t_n can be calculated from (2) by integration

$$\int_0^{t_n} dt = L \int_{i_n}^{I_{\rm ref}} \frac{di}{V_{in} - i r_i}$$

$$t_n = \frac{L}{r_i} \ln \left(\frac{\frac{V_{in}}{r_i} - i_n}{\frac{V_{in}}{r_i} - I_{\rm ref}} \right). \tag{6}$$

The final value of v_c is obtained by integrating the capacitor discharge (3)

$$v_c(t_n) = v_n e^{-t_n/(R+r_c)C} \tag{7}$$

and $v_c(t_n)$ should not be less than V_{in} if the model is to remain valid.

When switch is off, substituting i and di/dt from (5) into (4) we get a second-order differential equation of v_c in the form

$$\ddot{v}_c + \alpha_1 \dot{v}_c + \alpha_2 v_c = \alpha_3 \tag{8}$$

[1]If this condition is violated, i temporarily exceeds $I_{\rm ref}$ at the beginning of the off period. The model would fail if the next clock pulse arrives while i is still greater than $I_{\rm ref}$.

where

$$\alpha_1 = \frac{L + r_i C(R + r_c) + R r_c C}{LC(R + r_c)}$$

$$\alpha_2 = \frac{R + r_i}{LC(R + r_c)}$$

$$\alpha_3 = \frac{V_{in} R}{LC(R + r_c)}.$$

If the clock period is T, then t_n/T will count the clock pulses in the on period. The remainder part of it multiplied by T will give the time of switching off after the last clock pulse. Since the next switch on takes place at the arrival of the very next clock pulse, the off period t'_n is given by

$$t'_n = T\left[1 - \left(\frac{t_n}{T}\right) \bmod (1)\right]. \tag{9}$$

The general solution of the linear nonhomogeneous differential equation (8) is the sum of the solution of the corresponding homogeneous equation and a particular solution.

The particular solution is given by putting a final value $v_c = k$ in (8) after all derivative quantities become zero. So

$$k = \frac{\alpha_3}{\alpha_2} = \frac{V_{in} R}{R + r_i}.$$

The solution of the homogeneous equation has three different functional forms depending on the roots of the characteristic equation

$$\lambda_1 = -\frac{\alpha_1}{2} + \sqrt{\frac{\alpha_1^2}{4} - \alpha_2}$$

$$\lambda_2 = -\frac{\alpha_1}{2} - \sqrt{\frac{\alpha_1^2}{4} - \alpha_2}.$$

Case 1. $\alpha_1^2/4 > \alpha_2$*:* In this case, the two roots are real and distinct, and the solution of (8) is

$$v_c(t) = c_1 e^{\lambda_1 t} + c_2 e^{\lambda_2 t} + \frac{\alpha_3}{\alpha_2}. \tag{10}$$

Putting the initial condition for off condition, we get

$$c_1 = v_n e^{-t_n/(R+r_c)C} - \frac{V_{in} R}{R + r_i} - c_2$$

$$c_2 = \frac{1}{\lambda_1 - \lambda_2} \left[-\frac{V_{in} R}{R + r_i} \lambda_1 - \frac{R I_{\rm ref}}{C(R + r_c)} + v_n e^{-t_n/(R+r_c)C} \left\{ \lambda_1 + \frac{1}{C(R + r_c)} \right\} \right].$$

Let the output voltage at the next switch *on* instant be v_{n+1}, the current i_{n+1}. These are obtained as

$$v_{n+1} = c_1 e^{\lambda_1 t'_n} + c_2 e^{\lambda_2 t'_n} + \frac{V_{in} R}{R + r_i} \tag{11}$$

$$i_{n+1} = \frac{c_1}{R} [1 + C\lambda_1 (R + r_c)] e^{\lambda_1 t'_n} + \frac{c_2}{R} [1 + C\lambda_2 (R + r_c)] e^{\lambda_2 t'_n} + \frac{V_{in}}{R + r_i}. \tag{12}$$

Case 2. $\alpha_1^2/4 = \alpha_2$*:* In this case the solution of (8) is

$$v_c(t) = (c_1 + c_2 t)e^{-(\alpha_1/2)\,t} + \frac{V_{in}R}{R + r_i} \tag{13}$$

where

$$c_1 = v_n e^{-t_n/(R+r_c)C} - \frac{V_{in}R}{R + r_i}$$

$$c_2 = \frac{I_{\text{ref}}R + \{C\alpha_1(R + r_c)/2 - 1\}c_1 - V_{in}R/(R + r_i)}{C(R + r_c)}.$$

And the mapping from one switching instant to another is given by

$$v_{n+1} = (c_1 + c_2 t_n')e^{-(\alpha_1/2)\,t_n'} + \frac{V_{in}R}{R + r_i} \tag{14}$$

$$i_{n+1} = \frac{1}{R}\,[c_1 + c_2 t_n' + C(R + r_c)\{c_2 - c_1\alpha_1/2 - c_2\alpha_1 t_n'/2\}]e^{-(\alpha_1/2)\,t_n'} + \frac{V_{in}}{R + r_i}. \tag{15}$$

Case 3. $\alpha_1^2/4 < \alpha_2$*:* In this case, the oscillatory solution of the linear nonhomogeneous equation (8) is

$$v_c(t) = \exp\left(\frac{-\alpha_1}{2}\,t\right)[c_1 \cos \omega t + c_2 \sin \omega t] + \frac{V_{in}R}{R + r_i} \tag{16}$$

where

$$\omega = \sqrt{\alpha_2 - \frac{\alpha_1^2}{4}}$$

and the initial conditions give

$$c_1 = v_n e^{-t_n/(R+R_c)C} - \frac{V_{in}R}{R + r_i}$$

$$c_2 = \frac{I_{\text{ref}}R - c_1 + C\alpha_1 c_1(R + r_c)/2 - V_{in}R/(R + r_i)}{\omega C(R + r_c).}$$

The mapping is given by

$$v_{n+1} = e^{-\alpha_1 t_n'/2}[c_1 \cos\omega t_n' + c_2 \sin\omega t_n'] + \frac{V_{in}R}{R + r_i} \tag{17}$$

$$i_{n+1} = e^{-\alpha_1 t_n'/2}\left[\frac{c_1}{R} + C(1 + \frac{r_c}{R})(c_2\omega - \frac{\alpha_1 c_1}{2})\right]\cos\omega t_n' + e^{-\alpha_1 t_n'/2}\left[\frac{c_2}{R} - C(1 + \frac{r_c}{R})(\frac{c_2\alpha_1}{2} + c_1\omega)\right]\sin\omega t_n' + \frac{V_{in}}{R + r_i}. \tag{18}$$

Thus, v_{n+1} and i_{n+1} are given explicitly as functions of v_n and i_n in all the three cases.

Out of the three possibilities, the third one giving an oscillatory solution is the most important from a practical point of view. The normal design procedures, based on obtaining CCM and low output voltage ripple, usually give parameter values which satisfy this condition. If the parasitic elements r_c and r_i are ignored, the condition for oscillatory solution becomes

$$R > \sqrt{\frac{L}{4C}}.$$

Since this condition contains the value of load resistance, a boost converter can change from oscillatory mode to nonoscillatory mode during operation. Therefore, this mode must be included in the model of the system.

The condition for the different types of behavior divides the parameter space into two parts, and Case 2 occurs for specific combinations of parameters representing a surface in the parameter space. This condition has been included for the sake of completeness. The mapping for Case 2 would have importance if one considers the change of behavior as a parameter is varied smoothly across the condition surface, such as when obtaining a bifurcation diagram. For practical purposes, however, this condition would have little importance since a parameter combination falling exactly on the condition surface would be very unlikely.

It may be noted that the mapping derived here can locate only the peaks of the output voltage waveform. It maps the state of the system from one switch-on instant to the next and not in synchronism with the clock frequency. This map-based model can be used to predict the behavior of the system under different parameter combinations.

There is another way of representing the boost converter as a map—by sampling it in synchronism with the clock. The map-based model for this case would contain an "if" statement.

If $t_n \geq T$, the values of v_n and i_n at the next clock instant are given by

$$i_{n+1} = \frac{V_{in}}{r_i} - \left(\frac{V_{in}}{r_i} - i_n\right)e^{-(r_i/L)T} \tag{19}$$

$$v_{n+1} = v_n e^{-T/C(R+rc)}. \tag{20}$$

If $t_n < T$, the equations derived for v_{n+1} and i_{n+1} under Cases 1, 2, and 3 hold, with $t_n' = T - t_n$.

III. Bifurcation Phenomena of the Boost Converter

The operation of the boost converter can be seen from two points of view. Since the clock pulse has an externally determined periodicity, one can identify the system periodicity as the number of clock pulses in a period of the output waveform. This is how one analyzes a nonautonomous system. On the other hand, if one is concerned only with the observable state variables, one can define the periodicity as the repetitive behavior of the output waveform as seen in the phase space. One can thus view the system also as an autonomous system. In the first case, one would sample the system at the frequency of the clock pulse and obtain the Poincare section. The periodicity would be determined from this. We call it the "stroboscopic sampling." In the second case, one would identify the peaks of the output waveform of one of the variables, and determine the periodicity from that data. Since this is the same as sampling it at the switch-on instants, we call it the "switch-on sampling." In Section II, we derived the map-based model for these cases. We present here the bifurcation diagrams obtained from both these points of view.

The map-based model provides a fast and easy way of obtaining the bifurcation diagrams. We iterate the map starting from any initial condition, say (0, 0), and eliminate the initial

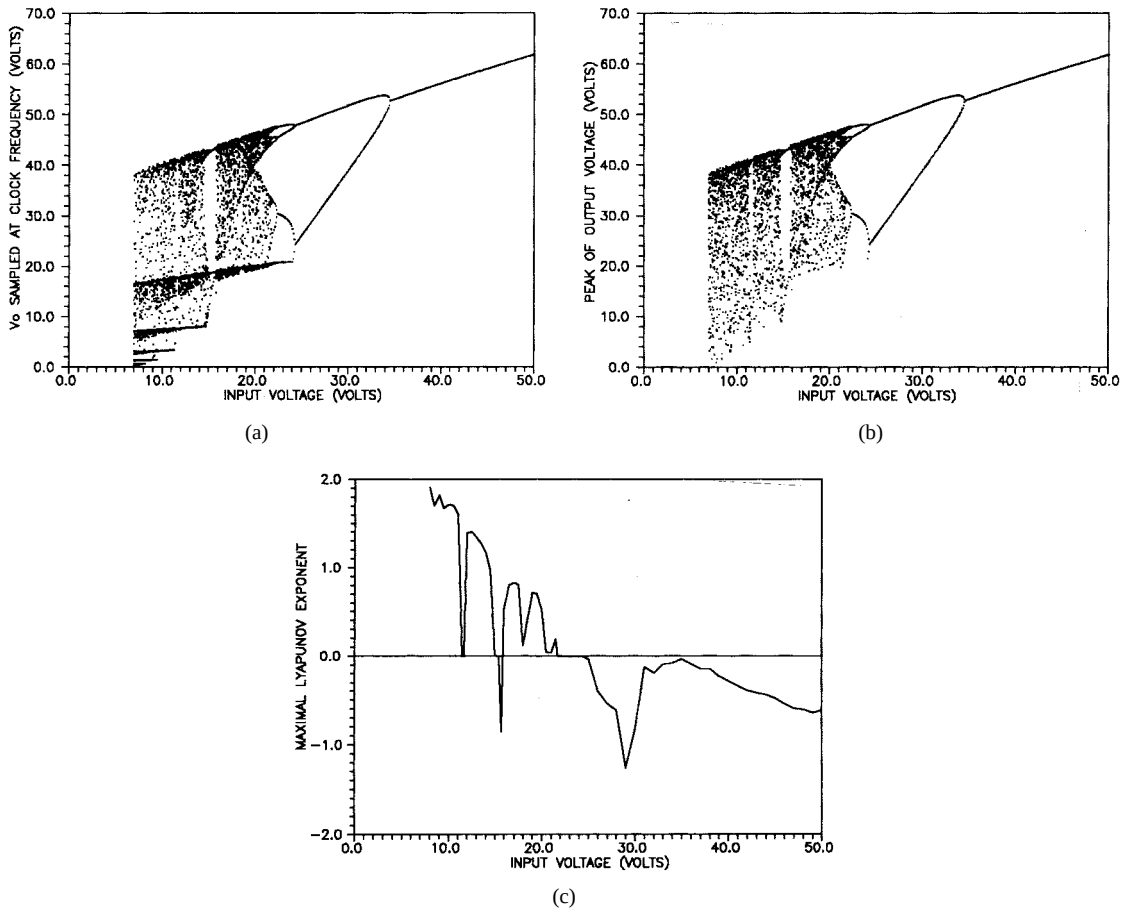

Fig. 4. Bifurcation diagram of the boost converter with input voltage as parameter: (a) stroboscopic sampling, (b) switch-on sampling, and (c) spectrum of the maximal Lyapunov exponent.

transient to obtain the asymptotic behavior of the system. We then vary a system parameter and plot about 500 consecutive values of one of the system variables against each parameter value. If the system is periodic, all the points would fall at the same position and we would see just one point for that parameter value. Higher periodicities would appear as the number of dots equal to the periodicity of the system. And for chaos (period infinity) we would get a smudge of dots, none of them falling on the other. In such a bifurcation diagram, one can clearly see the change of behavior as a parameter is varied.

There are six major parameters in the system: the input voltage, load resistance, inductance, capacitance, reference current, and clock frequency. In addition, there are the parasitics r_i and r_c. Since this is a dc circuit, the load is assumed to be purely resistive.

It may be noted that if the clock period is much less than the time constant $C(R+r_c)$, the fluctuation in the load voltage is very small and the system becomes effectively one-dimensional. Therefore, in order to illustrate the bifurcation behavior of the derived two-dimensional map, we have chosen the parameters such that T is comparable to $C(R+r_c)$.

In the following sections, bifurcation diagrams for variation of the above parameters are presented. One parameter is varied at a time with the others fixed at some nominal value. It is obvious that the bifurcation structures are dependent on these nominal parameter settings. However, since there are six parameters in the system, it is impossible to present these diagrams for all possible parameter values. We therefore present only a few typical cases.

A. V_{in} as the Bifurcation Parameter

The bifurcation diagram of the boost converter with input voltage as parameter is shown in Fig. 4. Fig. 4(a) shows the bifurcation diagram for stroboscopic sampling and Fig. 4(b) shows bifurcation diagram for the switch-on sampling. Fig. 4(c) shows the corresponding Lyapunov spectrum. Input voltage is varied from 7 to 50 V with a step of 0.1 V with other parameters fixed at $R = 20\ \Omega$, $C = 120\ \mu$F, $L = 27$ mH, $I_{\rm ref} = 4$ A, $r_i = 1.2\ \Omega$, $r_c = 0.1\ \Omega$, and clock frequency 500 Hz.

The boost converter shows period-doubling cascade from period 1 to chaos as input voltage is *decreased* from 50 V. The first bifurcation takes place at 34.9 V where the period 1 bifurcates to period 2. The period 2 behavior again bifurcates to period 4 behavior at 24.4 V.

It may be noted that the two diagrams start to show difference as input voltage is decreased below 24.3 V. This happens when a pulse arrives during the on time before the current reaches $I_{\rm ref}$. At this time there are four clock pulses in a cycle, though the orbit in the phase space is period 3.

As V_{in} is reduced below 21.8 V, the system enters chaos. This is confirmed by the fact that the maximal Lyapunov ex-

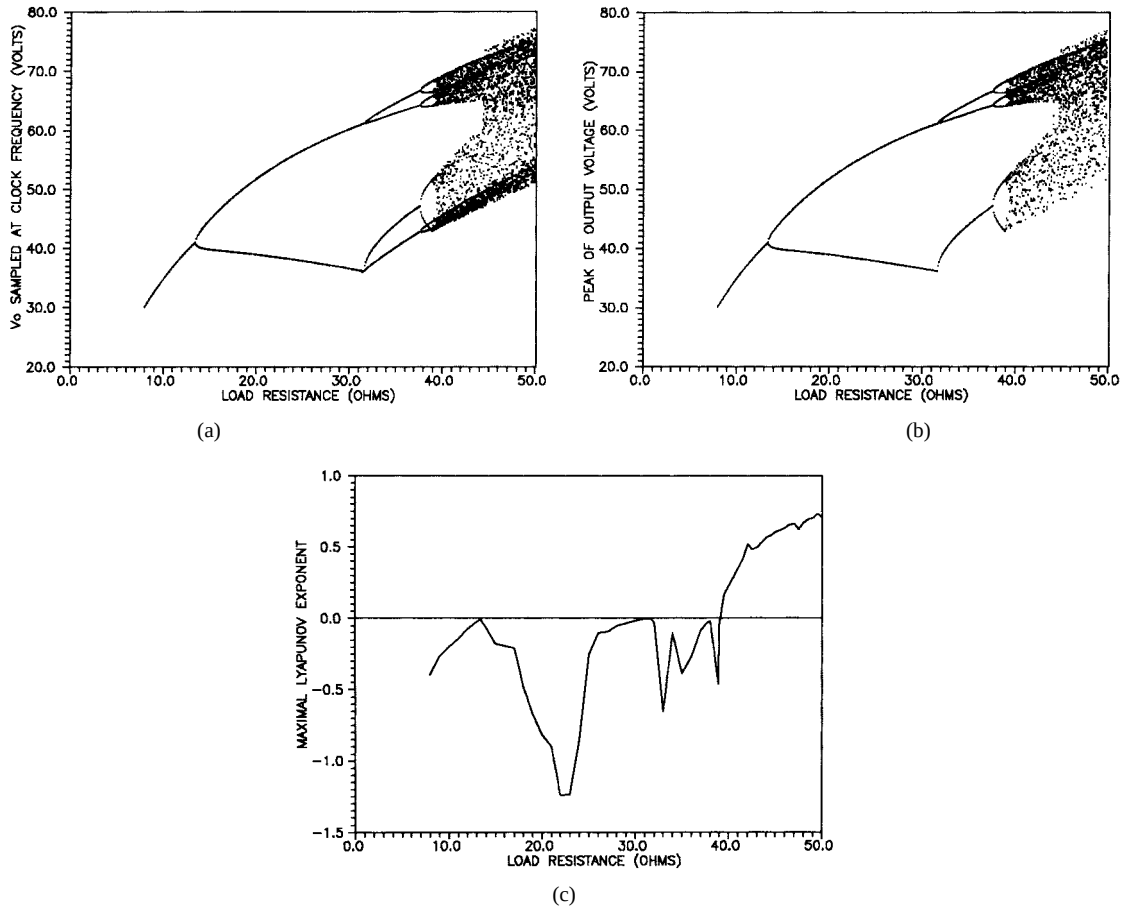

Fig. 5. Bifurcation diagram of the boost converter with load resistance as parameter: (a) stroboscopic sampling, (b) switch-on sampling, and (c) spectrum of the maximal Lyapunov exponent.

ponent becomes positive [Fig. 4(c)]. There are small periodic windows in the chaotic region, which also exhibit period-doubling cascade. The periodic windows embedded in the chaotic zone has a sequence of periods 3–6 in the voltage range of 15.7–15 V and periods 4–8 in the zone of 11.7–11.6 V. The first periodicities in these windows show period-adding cascade.

In Fig. 4(a), a staircase like structure appears in the chaotic region. The number of stairs increases with the decrease of input voltage. Two stairs are observed from 24.7 to 15.6 V. With decreasing input voltage, there is an increase of size of the attractor. As size of the attractor increases it captures one more clock pulse at 15.02 V, thus making the number of stairs three. This continues up to 11.42 V. Similarly four stairs are observed from 11.41 to 9.94 V, five from 9.93 to 8.85 V, and six from 8.84 to 8 V and so on.

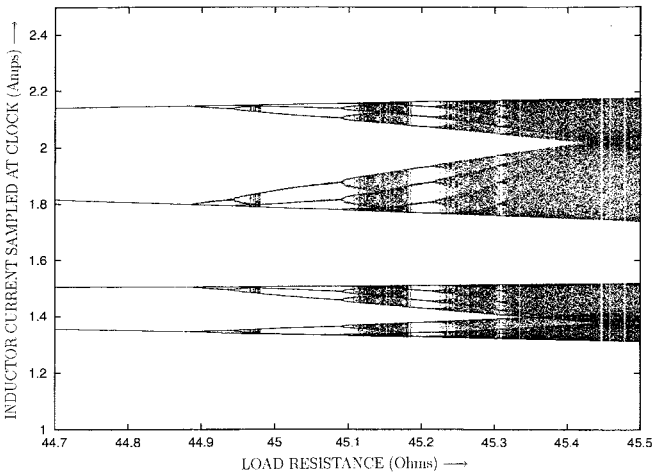

Fig. 6. Blowup of a portion of the chaotic region in Fig. 5, with inductor current as the observed variable.

B. R as the Bifurcation Parameter

The bifurcation diagram of the boost converter with load resistance as parameter is shown in Fig. 5. The load resistance is varied from 8 to 50 Ω with a step of 0.1 Ω while other parameters fixed at input voltage 30 V, reference current 4 A, capacitance 120 μF, inductance 27 mH, and clock frequency 500 Hz. Bifurcation and chaos are observed when load resistance is increased. Period 1 behavior is observed from 8 to 13.3 Ω. Period 1 bifurcates to period 2 at 13.4 Ω. This period 2 region exists up to 31.6 Ω. Up to period 2 region both the cases (i.e., stroboscopic and switch-on sampling) behave in the same way. At 31.7 Ω, the period 2 bifurcates to period 3 in the switch-on sampling and period 4 in the stroboscopic sampling. Starting from 31.7 Ω, one can observe four clock pulses in a complete cycle while in the output waveform the same state repeats after three loops. This behavior continues

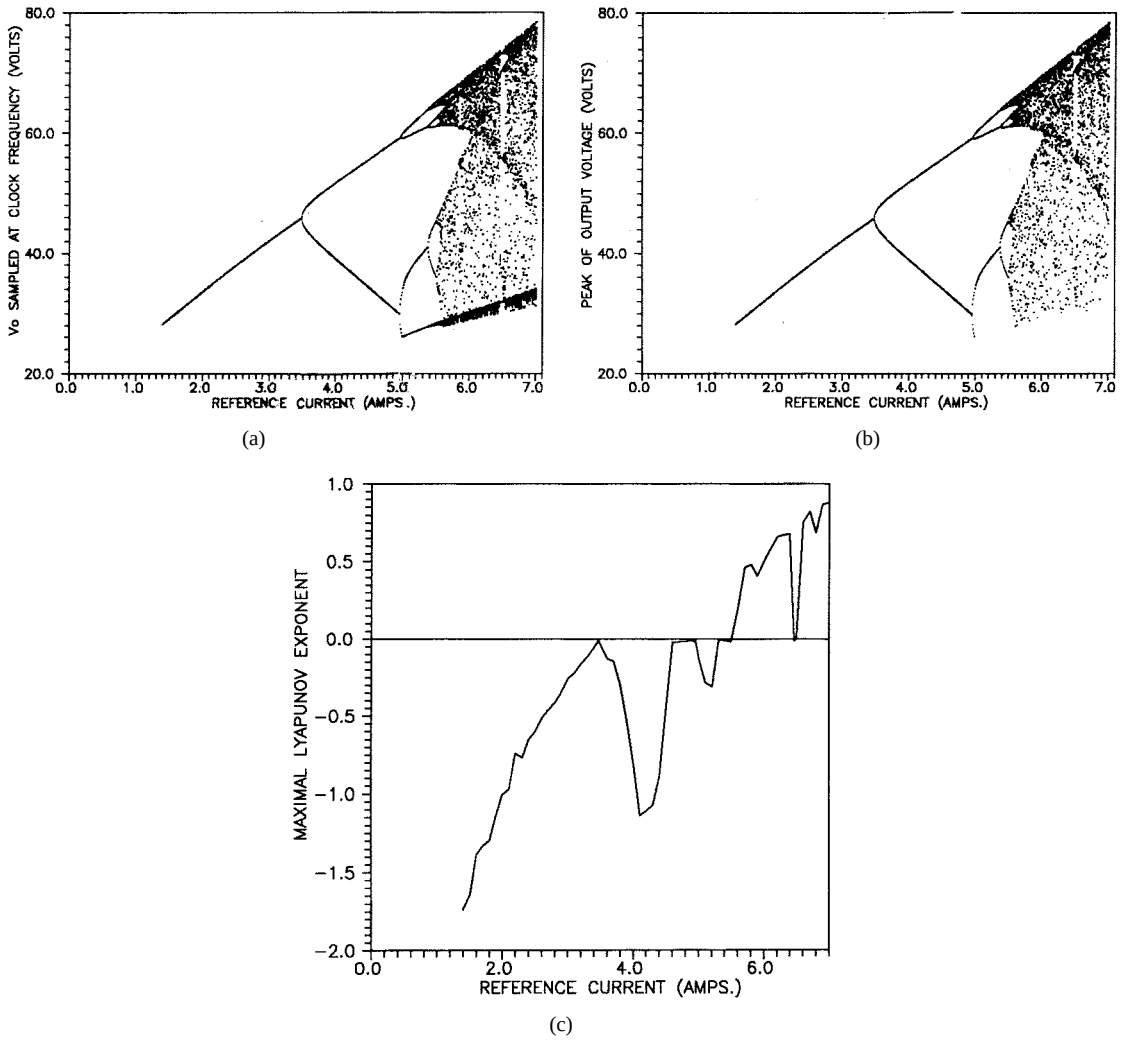

Fig. 7. Bifurcation diagram of the boost converter with reference current as parameter: (a) stroboscopic sampling, (b) switch-on sampling, and (c) spectrum of the maximal Lyapunov exponent.

up to load resistance of 37.6 Ω and then goes through period-doubling cascade to enter chaos.

A blowup of the chaotic region with i as observed variable is shown in Fig. 6. It shows that there are periodic windows that show period-adding cascade, and the width of the windows becomes progressively smaller at higher periodicities. Detailed analysis of such phenomena from bifurcation theory is beyond the scope of this paper and will be presented in a separate paper [10].

C. $I_{\rm ref}$ as the Bifurcation Parameter

The bifurcation diagram of the boost converter with reference current as parameter is shown in Fig. 7. The reference current is varied from 1.4 to 7 A with a step of 0.01 A with other parameters fixed at input voltage 30 V, load resistance 20 Ω, capacitance 120 μF, inductance 27 mH, and clock frequency of 500 Hz. These diagrams show clear period-doubling bifurcations at 3.46 and 4.94 A. At 5 A, the two viewpoints exhibit a difference as one clock pulse appears in every cycle that does not cause a switching. Chaotic behavior starts from 5.51 A and has periodic windows at higher values of reference current.

D. Inductance L as the Bifurcation Parameter

The bifurcation diagram of boost converter with inductance as parameter is shown in Fig. 8. The inductance is varied from 1 to 30 mH with step of 0.1 mH and other parameters fixed at load resistance 20 Ω, input voltage 20 V, capacitance 120 μF, reference current 4 A, and clock frequency of 500 Hz. Period 1 behavior is observed from 1 to 4.3 mH. Period 1 bifurcates to period 2 at 4.4 mH which lasts up to 11.4 mH. It is interesting to note that the two lines corresponding to period 2 behavior cross at around 6 mH, and at that point the system exhibits a period 1 behavior.

The period 4 region starts at 11.5 mH. After a very narrow region lasting up to 11.6 mH, the two diagrams begin to differ. Thereafter, the behavior is period 3 in the switch-on sampling and period 4 in the stroboscopic sampling. Chaotic behavior starts at 18 mH following a period-doubling cascade.

E. C as the Bifurcation Parameter

One has to exercise some caution when using the capacitance as the bifurcation parameter. This is because of the second assumption under which the map was derived. For low

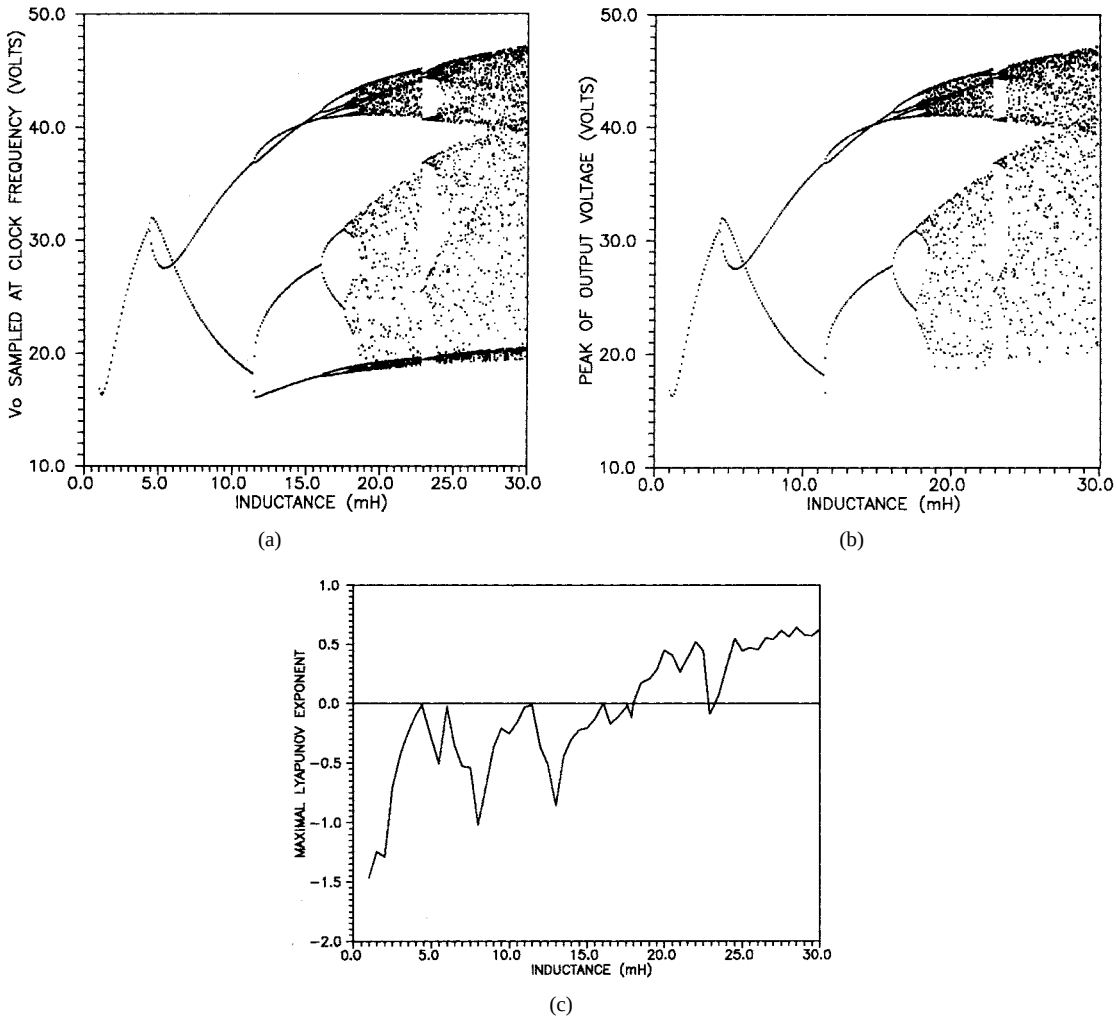

Fig. 8. Bifurcation diagram of the boost converter with inductance as parameter: (a) stroboscopic sampling, (b) switch-on sampling, and (c) spectrum of the maximal Lyapunov exponent.

values of the capacitance, the inductor current may shoot above the reference current for a part of the cycle, and the map-based model fails. One needs to keep track of the value of t_n, and if it goes negative the map-based model should not be used.

In order to avoid using two different kinds of models in two parts of the same bifurcation diagram, we have computed the bifurcation diagram from the continuous time model of the system while keeping a check on the continuity of inductor current. The capacitance was varied from 25 to 200 μF with a step of 0.1 μF. The input voltage and load resistance are kept constant at 20 V and 20 Ω, respectively, with other parameters fixed at inductance 27 mH, reference current 4 A, and clock frequency at 500 Hz. We find that the behavior is chaotic over the whole parameter range.

F. The Frequency of Clock as the Bifurcation Parameter

To investigate the change of system behavior with clock frequency, the frequency of the clock is varied from 500 Hz to 20 kHz with a step of 10 Hz with other parameters fixed at load resistance 20 Ω, capacitance 120 μF, inductance 27 mH, reference current 4 A, and input voltage 30 V. It is found that the clock frequency does not affect the topological property of the orbit qualitatively, though there are quantitative changes.

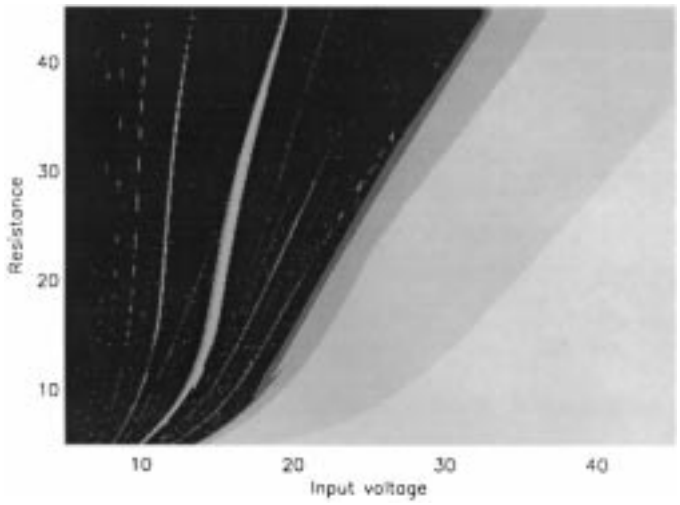

Fig. 9. Parameter space map of the boost converter showing regions of different periodicities with stroboscopic sampling. Darker shades imply higher periodicities.

For the parameter values chosen, the system remains chaotic throughout. This means that it is possible to increase or decrease the system frequency while maintaining the topological

orbital equivalence. The bifurcation diagram is not presented here for the sake of brevity.

G. The Effect of the Parasitic Elements

The parasitic elements r_i and r_c do not affect the bifurcation structures but they are found to shift the points at which bifurcation occurs when other major parameters are varied. For example, when load resistance is used as the bifurcation parameter, the period-doubling bifurcation occurs for a lower value of R if the inductor has a parasitic resistance. This justifies the inclusion of the parasitic elements in the model.

IV. The Parameter Space

The boost converter has two parameters namely input voltage and load resistance that can vary continuously during operation. The other parameters like inductance, capacitance and reference current are generally set at the design stage and are not assumed to be continuous variables. The boost converter may undergo bifurcations during operation depending on various combinations of the continuously varying parameters keeping others constant. It is therefore necessary to study the bifurcation patterns over the parameter space of V_{in} and R.

If the two parameters are shown in the two axes, it is not possible to draw bifurcation diagrams as in the earlier figures. In that case, it is customary to depict the asymptotic behavior of the system with a color over a grid of the parameter space. In order to facilitate reproduction in monochrome, we present the V_{in} versus R parameter space "map" in Fig. 9, with higher periodicities depicted with darker gray levels. The darkest shade implies chaos.

Using such parameter space maps the designer can place the nominal operating point away from behavior boundaries.

V. Conclusions

We have presented a discrete model of the boost converter including the parasitic elements, which can be used to obtain the evolution of the state variables starting from any initial condition. Observation of the state can be made at the switch-on instants or in synchronism with the clock frequency. The map-based models for both these cases have been derived.

The discrete model enables one to avoid numerical computation of the phase space orbit from the continuous time model. The map is therefore very useful in quick computation of system behavior.

It is shown that the boost converter exhibits a rich variety of bifurcation phenomena. There are both period doubling as well as period-adding cascades. Moreover the subharmonic periodicities as multiples of the clock frequency and the periodicities of the output waveform are different for most parameter combinations.

So long as there is one clock pulse between two switch-on instants, the bifurcation diagrams from the points of view of switch-on sampling and stroboscopic sampling are identical. They start to differ only when the *on* period contains more than one clock period. These parameter regions can be identified from the bifurcation diagrams.

Since a converter's behavior is expected to be robust against modest changes in parameters, the present study shows that there is a necessity of working out the bifurcation patterns in the parameter space at the design stage to place the nominal operating point away from boundaries marking different asymptotic behaviors.

Acknowledgment

The authors thank Dr. D. Hamill and Dr. J. Deane of the University of Surrey, U.K., for their helpful suggestions in improving the paper.

References

[1] J. R. Wood, "Chaos: A real phenomenon in power electronics," in *Appl. Power Electron. Conf.*, Baltimore, MD, 1989.
[2] J. H. B. Deane and D. C. Hamill, "Instability, subharmonics, and chaos in power electronic circuits," *IEEE Trans. Power Electron.*, vol. 5, pp. 260–268, 1990.
[3] D. C. Hamill, "Power electronics: A field rich in nonlinear dynamics," in *Nonlinear Dynamics of Electronic Systems*, Dublin, Ireland, 1995.
[4] J. H. B. Deane and D. C. Hamill, "Chaotic behavior in current-mode controlled dc–dc converter," *Electron. Lett.*, vol. 27, no. 13, pp. 1172–1173, 1991.
[5] J. H. B. Deane, "Chaos in a current-mode controlled boost dc–dc converter," *IEEE Trans. Circuits Syst. 1*, vol. 39, pp. 680–683, 1992.
[6] C. K. Tse, "Flip bifurcation and chaos in three-state boost switching regulators," *IEEE Trans. Circuits Syst. I*, vol. 41, pp. 16–23, 1994.
[7] K. Chakrabarty, G. Podder, and S. Banerjee, "Bifurcation behavior of buck converter," *IEEE Trans. Power Electron.*, vol. 11, pp. 439–447, 1995.
[8] F. D. Tan and R. S. Ramshaw, "Instabilities of a boost converter system under large parameter variations," *IEEE Trans. Power Electron.*, vol. 4, no. 4, pp. 442–449, 1989.
[9] D. C. Hamill and J. H. B. Deane, "Modeling of chaotic dc–dc converters by iterated nonlinear mappings," *IEEE Trans. Power Electron.*, vol. 7, no. 1, pp. 25–36, 1992.
[10] S. Banerjee, C. Grebogi, and E. Ott, "Border collision bifurcations: An explanation of the observed bifurcation phenomena in the boost converter," *IEEE Trans. Power Electron.*, to be published.

Soumitro Banerjee (M'91) was born in Calcutta, India, in 1960. He received the B.E. degree from Bengal Engineering College, Calcutta, in 1981, and the M.Tech. degree from the Indian Institute of Technology, New Delhi, India, in 1983. He then worked on power system applications of Superconducting Magnetic Energy Storage in the same Institute and completed the Ph.D. degree in 1987.

He was with the Indian Institute of Technology, Kharagpur, India, as a Lecturer from 1985 to 1990, an Assistant Professor from 1990 to 1997, and is currently an Associate Professor at the same institute. His current interests include bifurcation theory and chaotic dynamics. The chosen areas of application are electrical circuits in general and power electronic circuits in particular.

Krishnendu Chakrabarty was born in Shillong, India, in 1962. He received the B.E. degree in electrical engineering from the Regional Engineering College, Silchar, India, in 1985, and the M.E. degree in power electronics from Bengal Engineering College, Calcutta, India, in 1990. He received the Ph.D. degree from the Indian Institute of Technology, Kharagpur, India, in 1997.

He has served the Regional Engineering College, Silchar, India, as Lecturer from 1986 to the present. His areas of interest include bifurcation and chaos in power electronic circuits.